

A Novel UPF Rectifier for a Stand-Alone Wind Energy Conversion System

**M Shamily Rathan**

M.Tech Student

QIS College of Engineering & Technology,
Ongole, Prakasam -Dist. A.P.**Dr. B. Venkata Prasanth**

Professor & H.O.D.

QIS College of Engineering & Technology,
Ongole, Prakasam -Dist. A.P.

ABSTRACT

This project presents a near-unity-power-factor front-end rectifier employing two current control methods, namely, average current control and hysteresis current control, is considered. This rectifier is interfaced with a fixed-pitch wind turbine driving a permanent-magnet synchronous generator. A traditional diode-bridge rectifier without any current control is used to compare the performance with the proposed converter. Two constant wind speed conditions and a varying wind speed profile are used to study the performance of this converter for a rated stand-alone load. The parameters under study are the input power factor and total harmonic distortion of the input currents to the converter. The wind turbine generator-power electronic converter is modeled in PSIM, and the simulation results verify the efficacy of the system in delivering satisfactory performance for the conditions discussed. The efficacy of the control techniques is validated with a 1.5-kW laboratory prototype, and the experimental results are presented.

Introduction

The Sun, wind, and tides are some of the alternative sources of energy that are used to generate power to overcome the limitations of conventional fossil fuels such as coal, natural gas, and oil. They are environmentally friendly and offer unlimited potential for utilization as they are available in abundance for free.

The generation of electric energy from wind systems has grown very quickly—from a global installed power of 4.8 GW in 1995 to 58 GW in 2005, at an average annual growth rate of 24%. As of 2011, it is estimated that 83 countries around the world use wind power on a commercial basis. Wind energy systems can be employed as either stand-alone systems or grid-connected systems. Power production closer to the load centers contributes to reduced costs and increased energy demand satisfaction. Since the majority of the literature related to small-scale wind turbine systems deals with grid-connected systems and the analysis presented cannot be extended to stand-alone systems, there is a need for study of wind energy as a principal power source for isolated sites, i.e., stand-alone wind systems

The focus of this work is on the front-end converter design for a stand-alone wind energy conversion system (WECS). Such a system design is relevant to locations where conventional generation is not practical or connection to the grid is not feasible. A very pertinent problem in such systems is that of harmonic generation and poor input power factor.

High levels of harmonic distortion in line currents and voltages reduce the overall system efficiency and lead to interference with the interdependent components, equipment malfunction, and high losses. A number of standards and regulations such as IEEE-519 and IEC

61000-3 have been introduced to determine permissible levels of harmonic content in currents that are injected into the utility grid.

The aim of the designed converter is to facilitate high-power factor operation and achieve acceptable harmonic content of input currents at the generator stator terminals and to extract the maximum possible real power at the permanent-magnet synchronous generator (PMSG)–power-electronic-converter interface. This has been achieved by employing two current control methods—the average current control (ACC) and hysteresis current control (HCC)—for the front-end rectifier. This rectifier is a three-phase converter employing three static bidirectional switches to perform line current shaping and ensuring high-input-power-factor operation. Insulated-gate bipolar transistors (IGBTs) are used in the construction of these switches because the power requirement is only a small fraction of the rectifier’s during the converter operation. This keeps the stresses on the switches low and enables the usage of low-power devices, leading to a significant reduction in cost.

Objective:

Main objective of this thesis is to design a suitable permanent magnet synchronous generator working with a vertical axis wind turbine. Wind energy conversion system consisting of above mentioned elements works on a variable speed principle. In small scale wind turbines, blade pitch mechanism usually is not applied.

Instead, a power electronics converter compensate variation for the wind variation and thus it contributes to high power coincident. The corresponding topology of PMSG is a surface mounted machine with concentrated winding. This type of winding suits for low speed applications since implementing high number of poles is easy. The major benefit of high pole numbers is eradication of gearboxes. Gearboxes result in lower availability of the entire system and they cause high amount of non-user friendly audible noise. Reduction of magnetic noise by the machine is targeted at the design stage. Additionally, the chosen topology can be easily

scaled by increasing the length of the machine. Of paramount, at the design stage, objective function is to reduce manufacturing expenses and cost of active material.

Wind Energy Systems

Wind system

Wind is a highly stochastic energy source. There is also a strong interdependence between the aerodynamic characteristics of the wind turbine, the generator’s rotor speed, and the amount of power that can be extracted from the wind. Hence, it becomes necessary to implement a control method that will enable the extraction of the maximum power from the system under all possible operating conditions. The following sections highlight the major components of a stand-alone WECS

General modelling of wind turbine

Wind turbines are classified based on the number of blades and the axis about which they are mounted. Typically, the three blade horizontal-axis wind turbine is preferred due to better performance as well as the even distribution of variations in ind speed from the rotors to the drive shaft. It is also capable of achieving better power coefficient

The output mechanical power of the wind turbine is given by the cube law equation

$$P_m = 0.5\rho C_p A U_w^3 \quad (\text{Watts}) \quad (1)$$

where ρ is the density of air (in $\text{kg} \cdot \text{m}^3$), C_p is the power coefficient, A is the area swept by the wind turbine rotor (in square meter), U_w is the wind speed (in meters per second). The power coefficient is a function of the tip speed ratio λ and the blade pitch angle β . It describes the efficiency of the wind turbine in converting the energy present in wind into mechanical power. The tip speed ratio λ may be defined as the ratio of the speed at which the outer tip of the turbine blade is moving to the wind speed. It is given by the equation

$$\lambda = (r\omega_m)/U_w. \quad (2)$$

The blade pitch angle β is defined as the angle at which the wind contacts the blade surface. The expression for power coefficient is given as

It is valid to assume pitch angle to be zero for low to medium wind velocities [9]. Hence, in this work, $\beta = 0^\circ$. To achieve maximum extraction of power from the system, the tip speed ratio and power coefficient have to be maintained close to the optimal values and varied according to the variations in the wind speed conditions. The mechanical torque of the system is given by the equation

$$T_m = P_m / \omega_m \text{ (N} \cdot \text{m)}. \quad (5)$$

Configurations of wind systems

There are many generator types which find application in a WECS, such as squirrel-cage induction generator, doubly fed induction generator (DFIG), and the PMSG. Of these, the last two are most popularly used in WECS. In this paper, a PMSG is used as the wind turbine generator (WTG) because of its compact size, higher power density, reduced losses, high reliability, and robustness. The most significant advantage is the elimination of the gearbox, in comparison to the DFIG.

Thus, the wind turbine can be directly coupled to the generator. Such systems are called direct drive systems and are most suitable for low-speed operating conditions. Owing to the bell-shaped nature of wind turbine power curves, the WTG is operated in the variable speed mode in order to achieve maximum power from the incident wind.

Wind Turbine Aerodynamics

The amount of the kinetic energy in the air flow can be determined based on the size of wind turbine and the wind speed. The elementary momentum theory gives an explanation of energy conversion in ideal circumstances. The amount of the kinetic energy of a fluid mass \dot{m} with a mass density ρ , moving at a velocity ϑ through the area A is

$$E = \frac{1}{2} \cdot \dot{m} \cdot \vartheta^2$$

and the mass flow is

$$\dot{m} = A \cdot \rho \cdot \vartheta$$

The power available in the wind is equal to the amount of energy yield passing per second.

$$P_{wind} = E \cdot \dot{m} = \frac{1}{2} \cdot \rho \cdot A \cdot \vartheta^3$$

It is obvious that a small variation in the wind speed influences the available wind power drastically. It was first in 1922, the German engineer Betz showed that

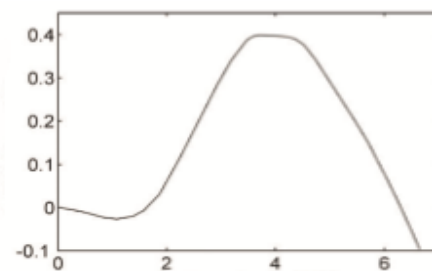


Figure 2.1. Power coefficient versus tip speed ratio].

the amount of extractable energy from an air stream is limited. It was shown that, in a free air stream, the maximum energy is extracted if the wind speed is reduced by three times far behind the turbine in comparison to in front of it. The maximum extractable power becomes then, 16/27 of available wind power.

For steady state analysis of aerodynamic conversion, a power coefficient diagram is used. As mentioned, it is not possible to capture all the power in the air flow as this would result in air standstill immediately after the wind turbine. Aerodynamic efficiency represents a ratio of captured power and available wind power. In wind power terminology, it is more known as the power coefficient. Betz factor is the maximum value for the power coefficient.

The power coefficient C_p is a function of the tip speed ratio λ and the blade pitch angle β . Equation 2.3 above, is modified according to equation 2.4.

$$P_{mech} = C_p \cdot P_{wind} = \frac{1}{2} \cdot \rho \cdot A \cdot C_p(\lambda, \beta) \cdot \vartheta^3$$

where

$$\lambda = \frac{r \cdot \omega}{v}$$

ω is the rotor tip angular speed and r is the rotor plane radius. Blade pitching means that the rotor blades are rotated along their axis, in order to control the amount of the absorbed power. In wind turbines which are not equipped with the control of the blade pitch, power coefficient is merely function of the tip speed ratio. Figure 2.1 shows a typical power coefficient diagram. Power coefficient is maximum at the optimum tip speed ratio i.e. in order to capture the maximum energy, the wind turbine rotor has to be run at this ratio. When the wind turbine rotor is run at other tip speed ratios, eddies will develop at the blade tip. This phenomenon reduces the captured energy and it is called stall. It explains the drop of the power coefficient at other tip speed ratios.

Wind Turbines

Wind turbines are categorised based on two different criteria; First due to their aerodynamic function; second based on their design. Considering the aerodynamic performance, wind turbines are divided into drag based and lift based. The rotors which utilise the drag force of the wind are recognised as slow speed turbines. However, in some turbines, the possibility of employing the lift force is also provided. The lift based turbines are recognised as high speed rotors. These are capable of capturing higher amount of the wind power compared to their drag based counterparts and therefore they are the most common solution today. Due to the second criterion, wind turbines are classified based on their axis of rotation. It is more common to distinguish wind systems as HAWT or VAWT.

HAWTs have benefited from technological advancements in the aircraft engineering because of the blades 'propeller like design. For instance, to achieve more lift forces, blade shapes' optimisation are proposed and applied. Power coefficients up to 0.5 of HAWT s have been reported. Today's VAWT s have reached power coefficient up to 0.4 at maximum. Figure 2.2 and Figure 2.3 show a H rotor VAWT and an installed HAWT respectively. Simplicity of the design of the

VAWT s is beneficial, especially the possibility to accommodate some of the drive train components on the ground together with absence of the yaw system 2. Some disadvantages of the system are the lower optimum tip speed ratio, inability to self start and inability to implement blade pitching for power control purposes. In some of the researchers' opinion the VAWT's power coefficient can exceed that of HAWT s' .

Working Principle of VAWT

Figure 2.4 shows a horizontal plan of a VAWT . The hub is assumed to be located at the centre of the coordinate system. The area with a positive value on



Figure 2.2. An H rotor VAWT .

Y-axis in Cartesian coordinate system is defined as up wind region and there maining area is defined as the downwind region. The angle of attack is the relative angle between the chord line of the blade cross section and the wind direction. This angle, seen by the blades in the upwind region, is negative. Since the angle of attack is negative, the lift force vectors produced on the blade section will point inwards the rotor. The force can be decomposed into two different components, a tangential and a normal. The former is along the tangent of the blade and the latter is perpendicular to the blade.

Moreover, the lift force will be created in downwind region. Here the angle of attack is positive, the consequent lift force vectors will point outwards the rotor. Tangential lift forces, originated from upwind and downwind regions, contribute to the torque production in the rotor. The normal force lead to thrust along the wind direction



Figure 2.3. A 450 kw HAWT with 37 m rotor diameter (Bonus).

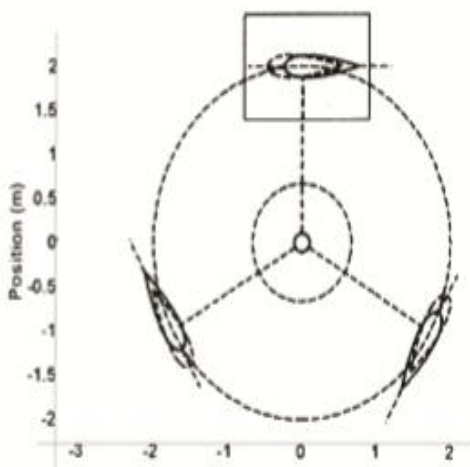


Figure 2.4. Horizontal plan of a VAWT

Electrical Machines for Wind Energy Systems Different Topologies of Electrical Machines

This chapter deals with different topologies of electrical machines for VAWT. In the text, Direct Current (DC) and induction generators precede synchronous generators. This chapter, furthermore, discusses "Design of a Permanent Magnet Synchronous Generator for a Vertical Axis Wind Turbine". Therefore the emphasis is put on various configurations of PMSG . In sections 3.2 and 3.3, different categories of PM synchronous machines are described. In section 3.4, implementable winding techniques with their effect on performance are given.

DC Generators

The application of DC generator in wind energy systems is not widely spread, mostly because of the high maintenance requirement of brushes and commutator and a need of a full scale inverter in order to get connected to the Alternative Current (AC) grid. Usually, DC generators are restricted to non-grid-connected wind energy systems with small DC loads, i.e. battery chargers.

Induction Generators:

Induction generator consumes reactive power which leads to a poor power factor of the machine. The power factor of smaller induction machines is lower compared to larger ones. The consumption of reactive power is penalized by many grid operators, since it causes losses in the grid. Some solutions are offered for active or passive compensation of reactive power. They include capacitor banks or condensers. Hence these solutions are costly.

Fixed Speed

Fixed speed wind energy systems including conventional Squirrel Cage / Short Circuit Induction Generator (SCIG) and a gearbox have been in use for decades. A big advantage is simplicity in operation and control of the system, however, there are also some disadvantages. In general, the wind is gusty and turbulent particularly in urban areas, which very often varies the speed of the

rotor and as a result a lower average efficiency is gained. Normally, dynamic disturbances are unavoidable in operation of the wind systems. They can occur in the turbine, e.g. variation in the shaft power, and in the grid, e.g. short circuits. However, in fixed speed systems the damping is low. Disturbances from the turbine and the grid influence each other harshly. Inrush current is, furthermore, an issue in wind systems with large induction machines. Figure 3.1 shows a block diagram of a typical fixed speed wind system including conventional SCIG gearbox and a transformer.

Multi speed IG is suggested for improving the average efficiency in areas with gusty and turbulent winds. An electrical machine with usually two speed steps is chosen. First step works in partial load conditions with low wind speeds while the second works in full load conditions with high wind speeds. There are different ways of such a system implementation. One solution, which also is the simplest one, is to have one IG with two different windings and two different numbers of poles. The second and more common solution is to utilise two induction machines. In both implementations, it will be possible to improve the average efficiency as well as the average power factor. The latter solution has been used in Danish wind systems during 80s and 90s [13]. Still, a complicated control system for switching between the steps remains an issue. Furthermore, cost of two windings in the former solution and cost of two IGs in the latter makes the multispeed wind systems more expensive.

Double Fed Induction Generator:

Double Fed Induction Generator (DFIG) is a variable speed wind system including induction machine where also the rotor is connected to the grid. Part of the power is either provided from the grid or delivered to the grid through the rotor. This power is called the slip power. Frequency of the slip power is varied in such a way that the rotor field frequency is maintained constant. Variation of the frequency of the slip power is established by means of two power electronics back to back converters. Bidirectional flow of the power in the

back to back converters gives the opportunity to work in sub synchronous mode as well as over synchronous mode. Back to back converter in DFIG consists of one machine-side-converter, a DC link capacitor and a grid-side-converter. Role of the machine-side-converter is to control the speed or the torque of DFIG and the machine power factor, while

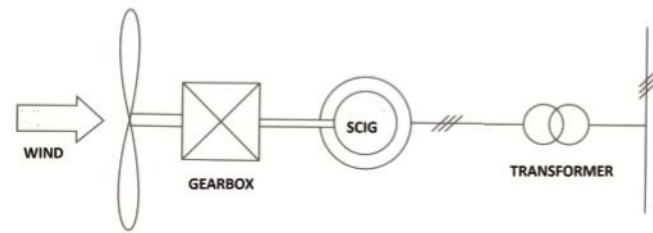


Figure 3.1. Block diagram of a fixed speed wind energy system including a conventional SCIG, a gearbox and a transformer.

the role of the grid-side-converter is to minimise DC link capacitor's voltage ripple. Figure 3.2 shows block diagram of a typical DFIG including a transformer. The benefit with this solution is the possibility of utilisation of conventional induction generators in a wider speed range and still obtain high efficiency. Because the converter is connected to the rotor, it only has to carry part of the power instead of entire rated power. Thus, the converter in DFIG is dimensioned in accordance to the required speed range. Usually the operating speed range does not exceed $\pm 40\%$ of the synchronous speed. In most of the wind systems on the market today, this is $\pm 30\%$. In, it has been shown that the converter rated at 30% of generator rated power is adequate for control of wind turbine rotor within a reasonable speed range. In other applications which will be introduced later on, the converter is dimensioned for the full power. Thus the cost and the losses of the converters in DFIG are lower in comparison to full power converters. This might be an issue for large wind systems. Other advantage is that the reactive power can be controlled independently from the active power. It means that DFIG can operate close to the unity power factor. The drawbacks with conventional DFIGs with gearbox are :

- High maintenance due to the slip rings.
- Limited capability of supplying reactive power.

- High torques in the machine during faulty conditions.
- Additional measures are required to limit the start-up current.

Moreover, the most complex control, especially regarding converters in wind systems are related to DFIG, which makes them essentially more economical for large wind systems rather than small systems.

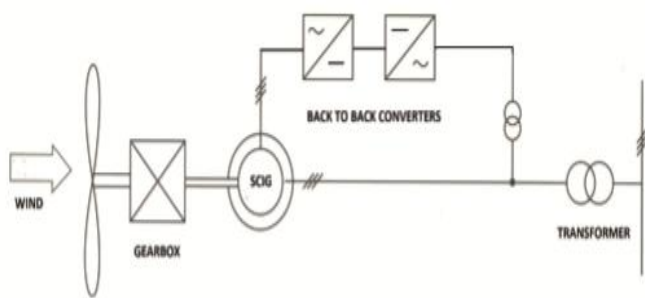


Figure 3.2. Block diagram of a typical DFIG including a transformer

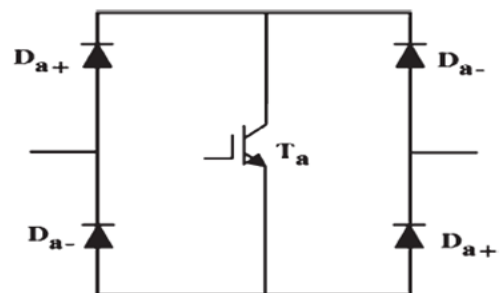
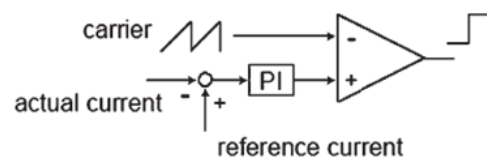
PROPOSED CONTROLLING METHODS

In most existing small-scale wind turbine systems, the preferred choice for a front-end converter is a diode-bridge rectifier because of its inherent simplicity.

However, due to their nonlinear nature, diode-bridge rectifiers inject harmonic components into the system, leading to an increased total harmonic distortion (THD) of input current, which is expressed as increased losses due to heating, malfunction of equipment, and reduced overall efficiency of the system. Along with input current THD, the PMSG operating power factor is another parameter of interest. If the PMSG operates at a lagging power factor, it leads to production of reactive power at the stator terminals, thereby reducing the maximum usable (real) power that the generator is capable of producing. Hence, it is desirable that the front-end converter is capable of maintaining high power factor and good quality currents, i.e., show good current control ability. The converter employed in this work, based on a topology suggested by Mehl and Barbi [18], is shown in Fig. 1. The selection of line inductance values (L_a , L_b , and L_c) plays a critical role in

maintaining unity-power-factor (UPF) operation and is defined as the sum of source inductance and the transformer leakage reactance [19], [20]. In a transformer-less system, the value of line inductance is based on the PMSG stator inductance alone. It employs a diode-bridge rectifier with three current-controlled static bidirectional switches. If the bidirectional switch connected to a particular phase is turned on, the corresponding phase is connected to the voltage central point, causing a rise of the associated phase current. Turning off the switch leads to conduction of the associated diode in the upper or lower half bridge (depending on the direction of current flow) and, therefore, to a reduction of the phase current.

Thus, the switching of the bidirectional switches enables us to achieve the possibility of a sinusoidal line current control (improved power factor). Maswood and Fangrui proposed a number of modifications to this topology in [21], where actual variations in load level on the rectifier were taken into account.



The dc link has two identical capacitors with a mid-point connection to the current control circuit, to maintain the voltage balance. The bidirectional switches are typically assembled using four diodes and an IGBT, as shown in Fig. 2. The voltage stress across the bidirectional switches in this topology is clamped to half of the dc output voltage by the dc-link capacitors, without the need for additional clamping circuits. This provides a

significant advantage over a single-switch boost topology, which suffers from the problem of high-voltage and high-current stresses across the single switch.

D. ACC Method

The average current controller employs the ramp comparison method. The instantaneous current error is calculated and fed to a proportional-integral (PI) regulator, as shown in Fig. 3. The output of the PI regulator is fed to a comparator along with a saw-tooth carrier. If intersections are obtained, the error is forced to remain within the band specified by the carrier waveform which is common to all the three phases. The integral term reduces the steady-state error between the reference and actual currents. Referring to Fig. 1, the following equations have been obtained:

$$\begin{cases} L(di_a/dt) = v_a - (v_{AM} + v_{MO}) \\ L(di_b/dt) = v_b - (v_{BM} + v_{MO}) \\ L(di_c/dt) = v_c - (v_{CM} + v_{MO}) \end{cases} \quad (6)$$

where i_a , i_b , and i_c are the inductor currents; v_a , v_b , and v_c are the source voltages from the PMSG; v_{MO} is the voltage of mode M in reference to the neutral point N; v_{AM} , v_{BM} , and v_{CM} are the voltages at nodes A, B, and C referring to node M. These voltages can be expressed as follows, where $sign(i_a)$, $sign(i_b)$, and $sign(i_c)$ depend on the polarity of inductor currents:

$$\begin{cases} v_{AM} = sign(i_a)(1 - s_a)(V_{dc}/2) \\ v_{BM} = sign(i_b)(1 - s_b)(V_{dc}/2) \\ v_{CM} = sign(i_c)(1 - s_c)(V_{dc}/2). \end{cases} \quad (7)$$

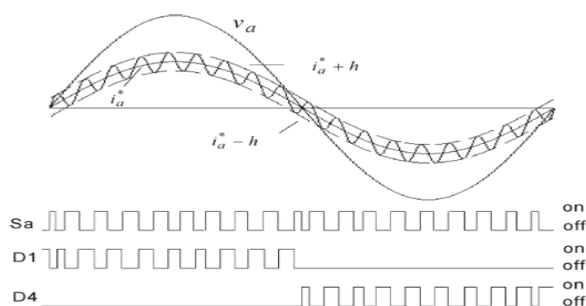


Fig. 4. Switching operation for phase “a”: Sa is the bidirectional switch for phase “a,” and D1 and D4 are the upper and lower bridge diodes, respectively.

For example,

$$sign(i_a) = \begin{cases} 1, & \text{if } i_a \geq 0 \\ -1, & \text{if } i_a < 0. \end{cases}$$

Here, s_a , s_b , and s_c are the switching states for the three bidirectional switches Sa, Sb, and Sc. “1” is for switch-on, and “0” is for switch-off. An outer dc voltage regulator has been implemented to maintain the dc-link voltage balance across the capacitors. However, there is a condition which states that, when half of the dc-link voltage is lesser than the phase voltage, the high-power-factor condition is not achieved

**E. HCC Method
Hysteresis Current Control**

The current control strategy plays an important role in the development of shunt active filter. The hysteresis-band current control method (Anshuman shukla et al 2007) is popularly used because of its simplicity in implementation. Hysteresis current controller derives the switching signals of the inverter power switches in a manner that reduces the current error. The switches are controlled asynchronously to ramp the current through the inductor up and down so that it follows the reference. The current ramping up and down between two limits is illustrated in Figure 2.2. When the current through the inductor exceeds the upper hysteresis limit, a negative voltage is applied by the inverter to the inductor. This causes the current through the inductor to decrease. Once the current reaches the lower hysteresis limit, a positive voltage is applied by the inverter through the inductor and this causes the current to increase and the cycle repeats. The current controllers of the three phases are designed to operate independently. They determine the switching signals to the respective phase of the inverter.

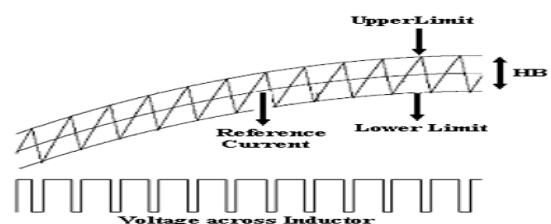


Figure 2.2 Hysteresis Current Control Operation Waveform

This method has the drawbacks of variable switching frequency, heavy interference between the phases in case of three phase active filter with isolated neutral and irregularity of the modulation pulse position. These drawbacks result in high current ripples, acoustic noise and difficulty in designing input filter. In this chapter, a constant frequency hysteresis current controller is proposed for shunt active filter applications. The details of the proposed current control strategy are presented in the next section.

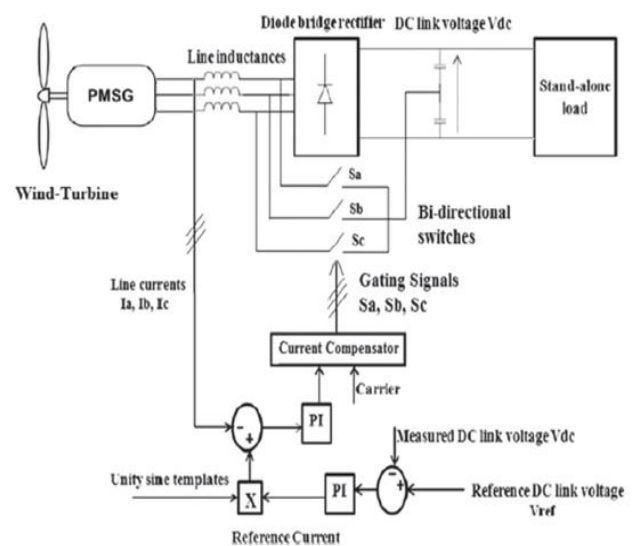
CONVERTER TOPOLOGY

A traditional wind system typically employs an uncontrolled diode-bridge rectifier-inverter system. It shows a vast degradation in performance under varying wind conditions. The line current at the input of the traditional rectifier exhibits very high harmonic distortion, contributing to increased losses and poor power factor at the PMSG-rectifier interface. This implies that the power extracted by the traditional ac-dc-ac converter is lower than the rated power of the wind-turbine-PMSG system. This highlights the importance of a current control method to ensure good power extraction, improved quality of current and voltage waveforms, and high efficiency. Thus, in this work, the diode rectifier is replaced with a front-end converter employing current control methods for efficient real power extraction.

The schematic of the wind-turbine-driven PMSG interfaced with the near-UPF converter employing the ACC method is shown in Fig. 5. Three bidirectional switches are connected between the input of the converter and the common point at the dc bus link at the output of the converter feeding a standalone load. In this paper, the stand-alone load is modeled as a sinusoidal pulsewidth-modulation (PWM) inverter connected to a star-connected three-phase load, described in the Appendix. The wind turbine is modeled according to (1)-(5). The input and output of the wind turbine block are the wind speed and the mechanical torque T_m , respectively. Mechanical torque T_m is the input to the PMSG block. I_a , I_b , and I_c are the generator currents

which are the input line currents to the front-end rectifier.

In the ACC method, the unity sine current templates are generated, which are compared with the actual line currents to get the error. This instantaneous error is fed to the PI regulator whose parameters need to be chosen carefully. The ramp comparison method is performed to generate the gating signals S_a , S_b , and S_c for the switches. The schematic employed for the HCC is shown in Fig. 6, where the unity sine references are then sent to the hysteresis current controller along with the actual phase currents to generate switching signals for the three switches.



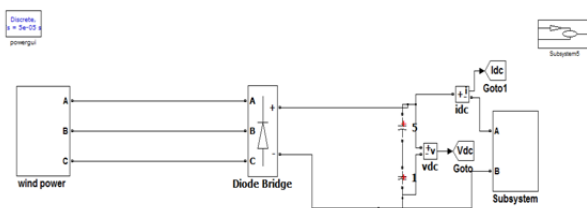
A phase-locked loop or phase lock loop (PLL) is a control system that generates an output signal whose phase is related to the phase of an input signal. While there are several differing types, it is easy to initially visualize as an electronic circuit consisting of a variable frequency oscillator and a phase detector. The oscillator generates a periodic signal. The phase detector compares the phase of that signal with the phase of the input periodic signal and adjusts the oscillator to keep the phases matched. Bringing the output signal back toward the input signal for comparison is called a feedback loop since the output is "fed back" toward the input forming a loop.

Keeping the input and output phase in lock step also implies keeping the input and output frequencies the same. Consequently, in addition to synchronizing signals, a phase-locked loop can track an input frequency, or it can generate a frequency that is a multiple of the input frequency. These properties are used for computer clock synchronization, demodulation, and frequency synthesis.

Phase-locked loops are widely employed in radio, telecommunications, computers and other electronic applications. They can be used to demodulate a signal, recover a signal from a noisy communication channel, generate a stable frequency at multiples of an input frequency (frequency synthesis), or distribute precisely timed clock pulses in digital logic circuits such as microprocessors. Since a single integrated circuit can provide a complete phase-locked-loop building block, the technique is widely used in modern electronic devices, with output frequencies from a fraction of a hertz up to many gigahertz.

SIMULATION RESULTS AND ANALYSIS

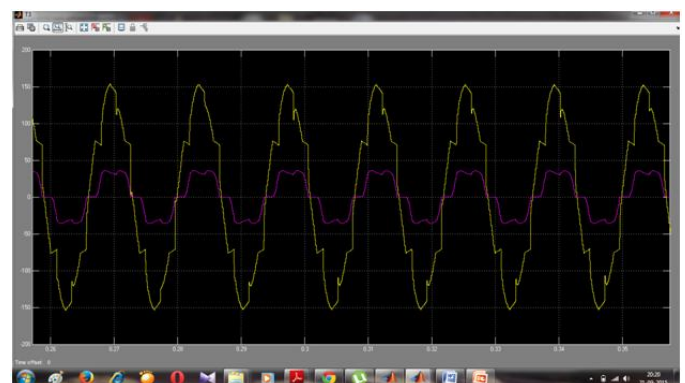
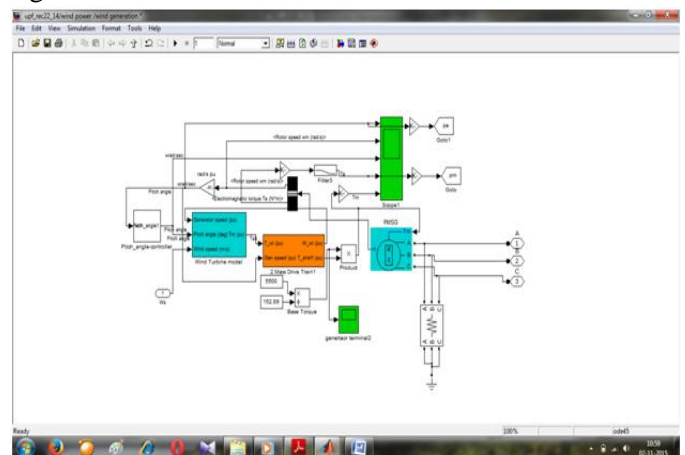
Performance of the System Without Current Control



In order to highlight the effect of a current-controlled frontend rectifier, the performance of the system utilizing an uncontrolled diode-bridge rectifier as the front-end converter was studied. A vast difference was observed in terms of the quality of currents as well as the real power extracted from the system. Fig. 13(a) shows the input phase voltage V_{an} and the corresponding phase current I_a for the WECS utilizing a front-end diode-bridge rectifier. The input power factor drops to 0.891. A reduced power factor implies a reduction in the real power extracted from the generator when the other

factors remain unchanged. Fig. 13(b) shows the harmonic spectrum of the phase “a” current. FFT spectrum is restricted to 1.5 kHz because of the negligible harmonics beyond this range. The THD of this phase current is as high as 45.21%, which is not within the acceptable limits of the IEEE 519 standard.

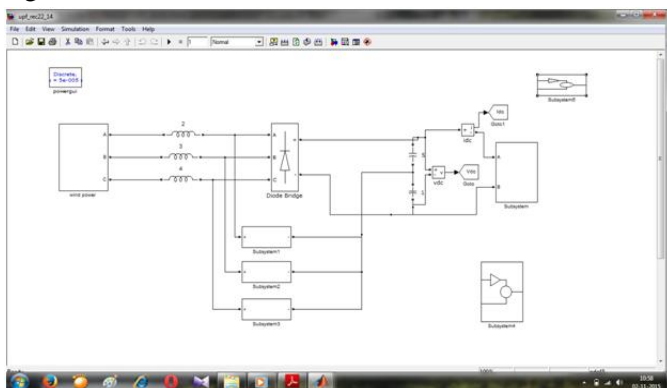
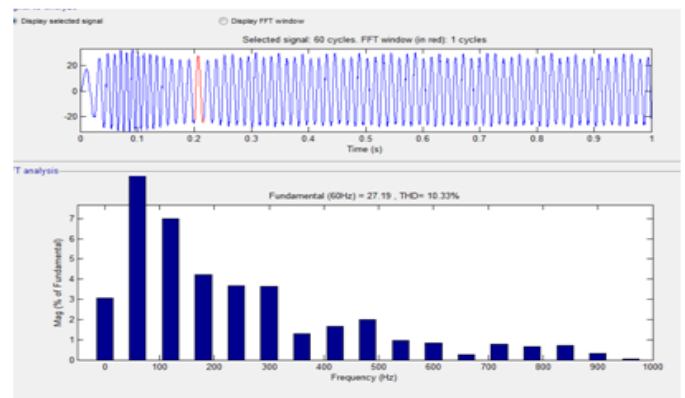
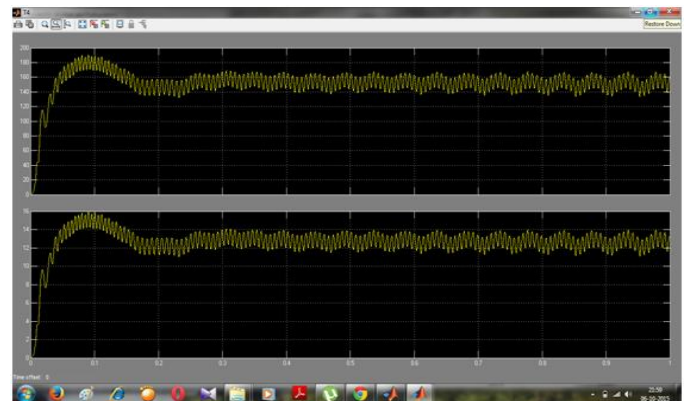
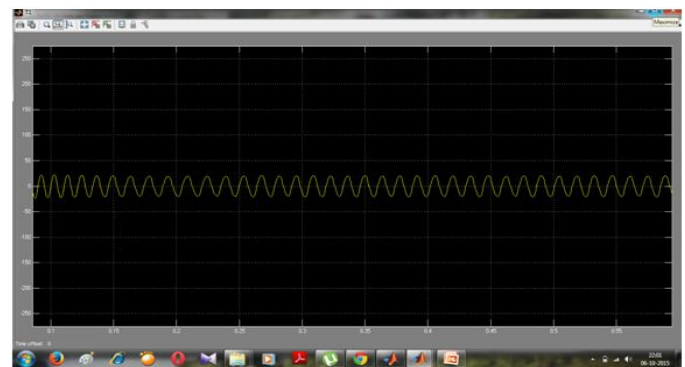
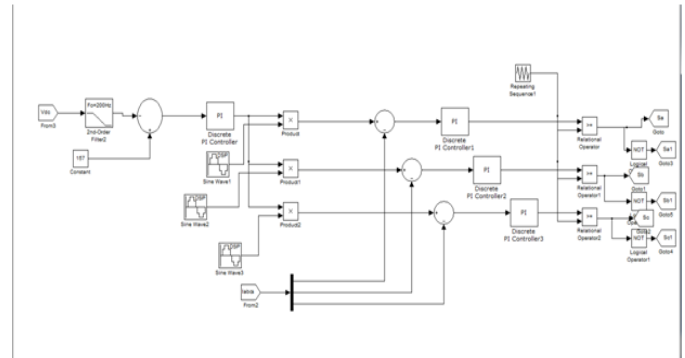
From Fig. 13(c), the mechanical power obtained from the wind turbine is 2.34 kW. The electrical power produced by the PMSG is 2.25 kW, which is transferred to the dc-link output of the front-end rectifier. Fig. 14 shows the change in coefficient of performance of the system in response to a sudden change in wind speed. Since the C_p is fluctuating widely, the steady-state average values are mentioned here. The performance coefficient reaches values of 0.445 and 0.468 for 12 and 14 m/s, respectively, which are lower than the corresponding C_p values with ACC and HCC. The need for current control methods is reinforced with these arguments.

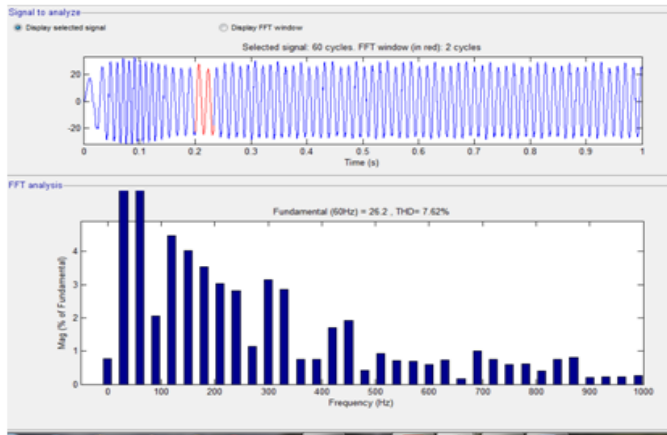


Performance of the System With ACC

The input voltage and current of phase “a” of the UPF rectifier. The quality of current and voltage is good, and the input power factor is high (0.994). Fig. 10(b) shows the FFT spectrum of phase “a” current. The fundamental frequency is at 36 Hz. The dominant components are close to 180 and 250 Hz, and their magnitudes are well below 10% of the fundamental current component’s magnitude. The THD of this current is 8.26%. The wind turbine mechanical power produced is 2.525 kW. The PMSG produces 2.47 kW, which is transferred entirely to the dc-link output, as can be seen in Fig. 10(c). Fig. 10(d) shows the voltages across the two output dc-link capacitors. The wind speed is increased to 14 m/s. Fig. 11(a) shows that the input power factor of the UPF rectifier is 0.994. Fig. 11(b) shows the dominant harmonics at 225 and 315 Hz. However, their magnitudes are lower than 10% of the fundamental’s magnitude. THD is calculated as 5.85%. Fig. 11(c) shows the system’s capability of extracting 97% of the available wind turbine power. The PMSG generates 3.9 kW, which is the input power available at the front-end rectifier.

This power is transferred entirely to the dc-link output of the rectifier, thus achieving high efficiency operation. While the voltage across the first capacitor is 195.4 V, the second capacitor has 193.3 V across it. The dc-link voltage achieved is 388.6 V in comparison to the reference value of 395 V. With a change in wind speed, the performance coefficient reaches values of 0.479 and 0.474 for 12 and 14 m/s, respectively, as can be seen in Fig. 12





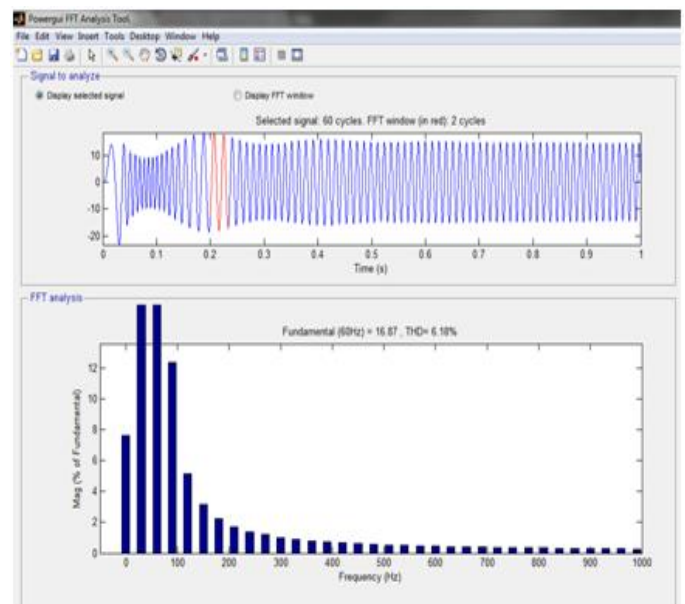
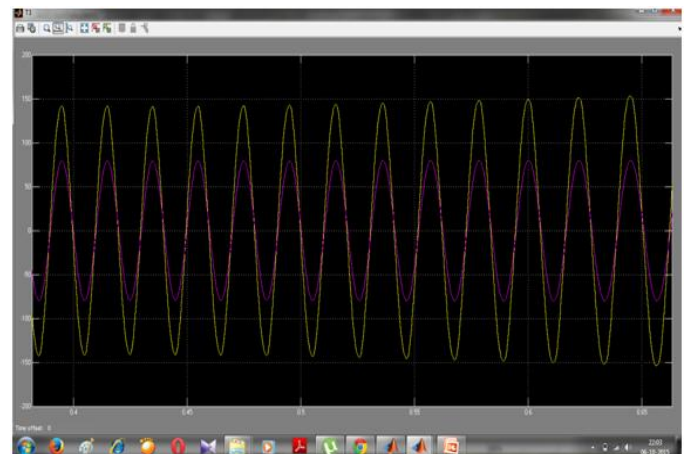
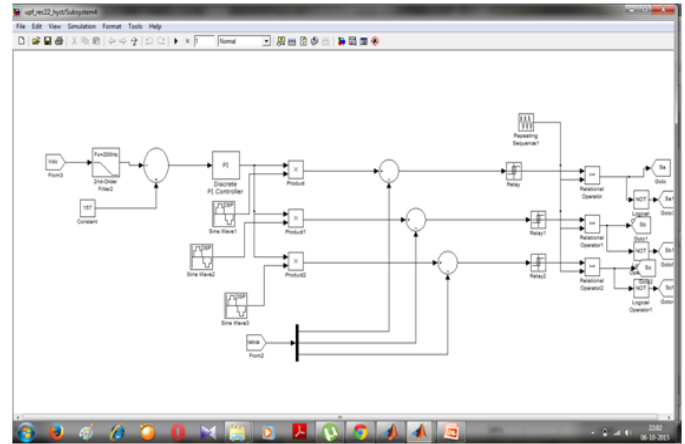
Performance of the System With HCC

In order to highlight the effect of a current-controlled frontend rectifier, the performance of the system utilizing an uncontrolled diode-bridge rectifier as the front-end converter was studied. A vast difference was observed in terms of the quality of currents as well as the real power extracted from the system. Fig. 13(a) shows the input phase voltage V_{an} and the corresponding phase current I_a for the WECS utilizing a front-end diode-bridge rectifier. The input power factor drops to 0.891. A reduced power factor implies a reduction in the real power extracted from the generator when the other factors remain unchanged.

Fig. 13(b) shows the harmonic spectrum of the phase “a” current. FFT spectrum is restricted to 1.5 kHz because of the negligible harmonics beyond this range. The THD of this phase current is as high as 45.21%, which is not within the acceptable limits of the IEEE 519 standard. From Fig. 13(c), the mechanical power obtained from the wind turbine is 2.34 kW. The electrical power produced by the PMSG is 2.25 kW, which is transferred to the dc-link output of the front-end rectifier.

Fig. 14 shows the change in coefficient of performance of the system in response to a sudden change in wind speed. Since the C_p is fluctuating widely, the steady-state average values are mentioned here. The performance coefficient reaches values of 0.445 and 0.468 for 12 and 14 m/s, respectively, which are lower than the corresponding C_p values with ACC and HCC.

The need for current control methods is reinforced with these arguments.



Conclusion

In this paper, a WECS interfaced with a UPF converter feeding a stand-alone load has been investigated. The use of simple bidirectional switches in the three-phase converter results in near-UPF operation. Two current control methods, i.e., ACC and HCC, have been employed to perform active input line current shaping, and their performances have been compared for different wind speed conditions. and further the performance can be improved with the Phased locked loop (PLL) and in future with the improved phased locked loop can be implemented for high levels of voltages and variable loads where phase locked loop is simple and reliable solution

The quality of the line currents at the input of the converter is good, and the harmonic distortions are within the prescribed limits according to the IEEE 519 standard for a stand-alone system. A high power factor is achieved at the input of the converter, and the voltage maintained at the dc bus link shows excellent voltage balance. The proposed method yields better performance compared to a traditional uncontrolled diode bridge rectifier system typically employed in wind systems as the front-end converter. Finally, a laboratory prototype of the UPF converter driving a stand-alone load has been developed, and the ACC and HCC current control methods have been tested for comparison. The HCC current control technique was found to be superior and has better voltage balancing ability. It can thus be an excellent front-end converter in a WECS for stand-alone loads or grid connection.

REFERENCES

- [1] Aditya Venkataraman, Student Member, IEEE, Ali I. Maswood, Senior Member, IEEE, Nirnaya Sarangan, and Ooi H. P. Gabriel, Student Member, IEEE "An Efficient UPF Rectifier for a Stand-Alone Wind Energy Conversion System" IEEE TRANSACTIONS ON INDUSTRY APPLICATIONS, VOL. 50, NO. 2, MARCH/APRIL 2014
- [2] Online. Available: http://en.wikipedia.org/wiki/Wind_energy
- [3] M. Druga, C. Nichita, G. Barakat, B. Dakyo, and E. Ceanga, "A peak power tracking wind system operating with a controlled load structure for stand-alone applications," in Proc. 13th EPE, 2009, pp. 1–9.
- [4] S. Kim, P. Enjeti, D. Rendusara, and I. J. Pitel, "A new method to improve THD and reduce harmonics generated by a three phase diode rectifier type utility interface," in Conf. Rec. IEEE IAS Annu. Meeting, 1994, vol. 2, pp. 1071–1077.
- [5] A. I. Maswood and L. Fangrui, "A novel unity power factor input stage for AC drive application," IEEE Trans. Power Electron., vol. 20, no. 4, pp. 839–846, Jul. 2005.
- [6] A. I. Maswood, A. K. Yusop, and M. A. Rahman, "A novel suppressed-link rectifier–inverter topology with near unity power factor," IEEE Trans. Power Electron., vol. 17, no. 5, pp. 692–700, Sep. 2002.
- [7] G. M. Masters, Renewable and Efficient Electric Power Systems. Hoboken, NJ, USA: Wiley, 2004.
- [8] V. Sheeja, P. Jayaprakash, B. Singh, and R. Uma, "Stand alone wind power generating system employing permanent magnet synchronous generator," in Proc. IEEE ICSET, 2008, pp. 616–621.
- [9] M. Singh and A. Chandra, "Control of PMSG based variable speed wind-battery hybrid system in an isolated network," in Proc. IEEE PES, 2009, pp. 1–6.
- [10] J. G. Slootweg, S. W. H. de Haan, H. Polinder, and W. L. Kling, "Modeling wind turbines in power system dynamics simulations," in Proc. IEEE Power Eng. Soc. Summer Meet., 2001, vol. 1, pp. 22–26.
- [11] P. C. Krause, O. Wasynczuk, and S. D. Sudhoff, Analysis of Electric Machinery. Piscataway, NJ, USA: IEEE Press, 1994.
- [12] N. Srighakollapu and P. S. Sensarma, "Sensorless maximum power point tracking control in wind energy generation using permanent magnet synchronous

generator,” in Proc. 34th Annu. IEEE IECON, 2008, pp. 2225–2230.

[13] N. A. Ahmed and M. Miyatake, “A stand-alone hybrid generation system combining solar photovoltaic and wind turbine with simple maximum power point tracking control,” in Proc. CES/IEEE 5th IPEDMC, 2006, pp. 1–7.

[14] T. Tafticht, K. Agbossou, A. Cheriti, and M. L. Doumbia, “Output power maximization of a permanent magnet synchronous generator based stand alone wind turbine,” in Proc. IEEE Int. Symp. Ind. Electron., Jul. 9–13, 2006, pp. 2412–2416.

[15] K. Tan and S. Islam, “Optimum control strategies in energy conversion of PMSG wind turbine system without mechanical sensors,” IEEE Trans. Energy Convers., vol. 19, no. 2, pp. 392–399, Jun. 2004.

[16] P. Hong-Geuk, J. Seok-Ho, L. Dong-Choon, and K. Heung-Geun, “Low cost converters for micro wind turbine systems using PMSG,” in Proc. 7th ICPE, 2007, pp. 483–487.

[17] D. S. Oliveira, M. M. Reis, C. Silva, L. Colado Barreto, F. Antunes, and B. L. Soares, “A three-phase high-frequency semi-controlled rectifier for PM WECS,” IEEE Trans. Power Electron., vol. 25, no. 3, pp. 677–685, Mar. 2010.

[18] E. L. M. Mehl and I. Barbi, “An improved high-power factor and low-cost three-phase rectifier,” IEEE Trans. Ind. Appl., vol. 33, no. 2, pp. 485–492, Mar./Apr. 1997.

[19] A. I Maswood and L. Keng Song, “Design aspects of planar and conventional SMPS transformer: A cost benefit analysis,” IEEE Trans. Ind. Electron., vol. 50, no. 3, pp. 571–577, Jun. 2003.

[20] A. I. Maswood and Z. Yoong, “Design aspects of a switch-mode transformer under wide input voltage

variation,” IEEE Trans. Ind. Electron., vol. 53, no. 3, pp. 752–758, Jun. 2006.